Journal of Alloys and Compounds 509 (2011) 2137–2142

Contents lists available at ScienceDirect

Journal of Alloys and Compounds

journal homepage: www.elsevier.com/locate/jallcom

Oxidation behavior of ignition-proof magnesium alloys with rare earth addition

J.F. Fan[a,b,*], Ch.L. Yang[c], G. Han[a,b], S. Fang[a,b], W.D. Yang[a,b], B.S. Xu[a,b]

[a] College of Materials Science and Engineering, Taiyuan University of Technology, Taiyuan 030024, PR China
[b] Key Laboratory of Interface Science and Engineering in Advanced Materials, Taiyuan University of Technology, Ministry of Education, Taiyuan 030024, PR China
[c] State Key Laboratory of Solidification Processing, Northwestern Polytechnical University, Xi'an 710072, PR China

ARTICLE INFO

Article history:
Received 6 June 2010
Received in revised form 23 October 2010
Accepted 27 October 2010
Available online 4 November 2010

Keywords:
Magnesium alloy
Selective oxidation
Rare earth

ABSTRACT

Ignition-proof magnesium alloy is obtained in Mg–Y–Ce system, which can be melted at 1173 K in air without any protections. A dense and compact oxide film is obtained on the surface of molten Mg–Y alloys when the concentration of Y is greater than 10 wt%. With the addition of Ce the critical concentration of Y in Mg–Y alloys for forming a protective film is decreased significantly from 10 wt% to 3 wt%. AES and XRD analysis reveal that the oxide film formed on the surface of Mg–3Y–4.5Ce alloy is mainly composed of Y_2O_3 and $Ce_{0.202}Y_{0.798}O_{1.601}$. Based on the theoretic analysis and experimental results, a selective oxidation model of Mg–Y alloys at high temperatures is developed, and the third-element effects of Ce in Mg–Y alloys are discussed in detail.

1. Introduction

Due to their high affinity to oxygen, Magnesium and its alloys are particularly prone to surface degradation during high temperature manufacturing stages such as melting, welding or heat treatment [1–3]. Commonly, Mg alloys are melted or processed under the atmospheres of the fluxes or gases (N_2, CO_2, SO_2, and SF_6) to avoid a potential fire hazard, diminish material loses and ensure quality of manufactured parts [4,5]. But the above methods have their inherent disadvantages such as environmental pollution, requiring complicated equipments and cost increase, et cetera. As a result, since the 1950s much interest has been focused on the investigation and development of ignition-proof Mg alloys [6–8]. According to F. Czerwinski, the oxidation process of AZ91D is divided into three periods: the protective layer, incubation and non-protective periods [9]. Small additions of Be, Ca have been proved to benefit the oxidation resistance of magnesium alloys, which can be ascribed to the formation of the dense film during oxidation [10–13]. You et al. investigated the increase of the oxidation resistance of Mg–Ca alloys for the formation of MgO/CaO protective film at elevated temperatures [10]. Zeng et al. ascribed that the addition of Be improved the oxidation resistance during alloying process [13]. However, ignition-proof Mg alloys with enough Be and Ca additions have not been extensively applied in industry due to their poor mechanical properties and the smart toxicity of Be. For these reasons, it is necessary to find new ignition-proof elements.

Rare earths are often used as addition elements to improve properties of materials; especially Y and Ce have been proved to improve oxidation and corrosion resistance [14–17]. Wang et al. investigated the early oxidation behaviors of Mg–Y alloys oxidized in pure O_2 at high temperatures, and the results showed that the oxidation behaviors of the Mg–Y alloys obeyed a parabolic law [16]. Liu et al. found that the corrosion rate of Mg–3Y alloy decreased in 0.1 M Na_2SO_4 attributed to a more protective surface film [14]. Our studies also revealed that the oxidation resistance of magnesium alloys could be improved by implanting rare-earth elements (Y, Ce) [18]. However, the oxidation mechanism of magnesium alloys is relatively complex and some physical phenomena are still not very clear. Therefore, it is necessary and also of interest to understand the oxidation behavior of magnesium alloys with addition of Y and Ce.

In the present research, the effect of Y and Ce additions on the oxidation behavior of Mg alloys at high temperatures was studied so as to provide a new idea for the preparation of ignition-proof Mg alloys. Moreover, a selective oxidation model of Mg–Y alloys was established and the third-element effect of Ce in Mg–Y alloys was analyzed.

2. Experimental procedures

All the alloys, i.e., Mg–Y and Mg–Y–Ce were prepared by commercial purity Mg (99.9 wt%), pure Y (99.3 wt%) and pure Ce (99.5 wt%) in a steel crucible under a cover gas mixture of CO_2 and SF_6. The chemical compositions of the resulting alloys and the oxidation films were analyzed using Inductively Coupled Plasma Atomic Emission Spectroscopy (ICP-AES) and Auger Electron Spectroscopy (AES). Samples about 20 mm × 20 mm × 5 mm were cut for ignition point testing in air

* Corresponding author at: College of Materials Science and Engineering, Taiyuan University of Technology, Taiyuan 030024, PR China. Tel.: +86 351 6014852; fax: +86 351 6010311.
E-mail address: fanjianfeng77@hotmail.com (J.F. Fan).

0925-8388/$ – see front matter © 2010 Elsevier B.V. All rights reserved.
doi:10.1016/j.jallcom.2010.10.168

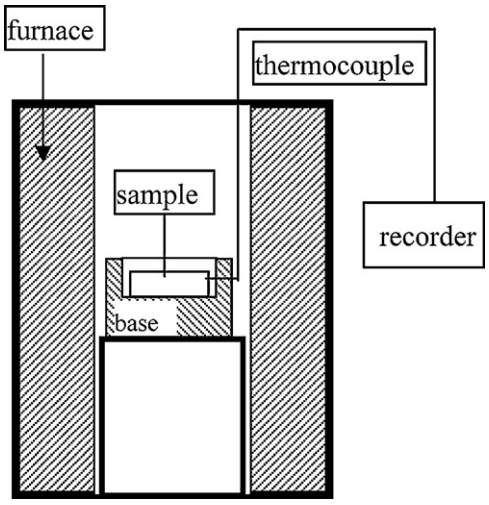

Fig. 1. The schematic diagram of ignition point testing device.

immediately after mechanical polishing and degreasing in acetone. The crystallographic features were examined mainly by X-ray diffraction with a Cu Kα source. The analyses of microstructure morphologies were accomplished by using a scanning electron microscope which was equipped with an energy dispersive spectrometer (SEM-EDS).

3. Results

3.1. Ignition points testing

Fig. 1 is the schematic diagram of ignition-point-testing device, which was heated in air at a rate of 4 K/min in the present experiment. The typical temperature vs. time curve of Mg in air is shown in Fig. 2. The combustion heat is large enough to cause a steep rise in the temperature–time curve of the samples, which proves the feasibility of the ignition-point-testing method used in this paper. Here the temperature located at the inflexion of the temperature–time curve is defined as the ignition point of Mg alloy. In Fig. 2, the vertical increase changes with the sizes of samples, and the larger the sample is, the higher the vertical increase is. So the definite value of the vertical increase is not given here.

The results of the ignition-point tests are shown in Fig. 3, in which 1173 K is the highest testing temperature. It can be seen that there is a threshold value (7 wt%) of Y contents in the curve of Y contents vs. the ignition points of Mg–Y alloys (Fig. 3a). When the Y contents are less than 7 wt%, the ignition points of Mg–Y alloys scarcely change compared with that of pure Mg, but when the Y contents are more than 7 wt%, the ignition points of Mg–Y alloys increase obviously. When the Y contents increase continuously and are more than 10 wt%, Mg–Y alloys will not burn hold at a high temperature 1173 K for 0.5 h. However, alloys with higher Y contents are uneconomic because of their high cost. In order to reduce the Y content in Mg–Y ignition proof alloys, cerium was added into Mg–Y alloys as a third element. Fig. 3b indicates that the effect of Ce additions on the ignition points of magnesium alloys is very small. However, to our surprise, when Y and Ce are added together into Mg alloys, the ignition points of Mg alloy increase rapidly. Fig. 3c shows the effect of Ce on the ignition points of Mg–3 wt% Y alloys. It is obvious that the ignition proof properties of Mg–Y–Ce alloys are excellent while the Y content is decreased significantly from 10 wt% to 3 wt%.

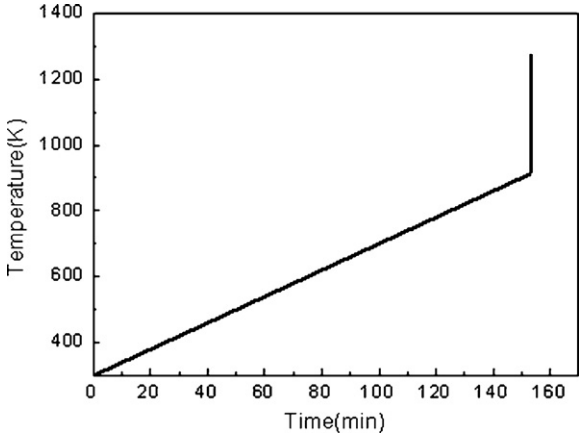

Fig. 2. The typical temperature vs. time curve of Mg in air.

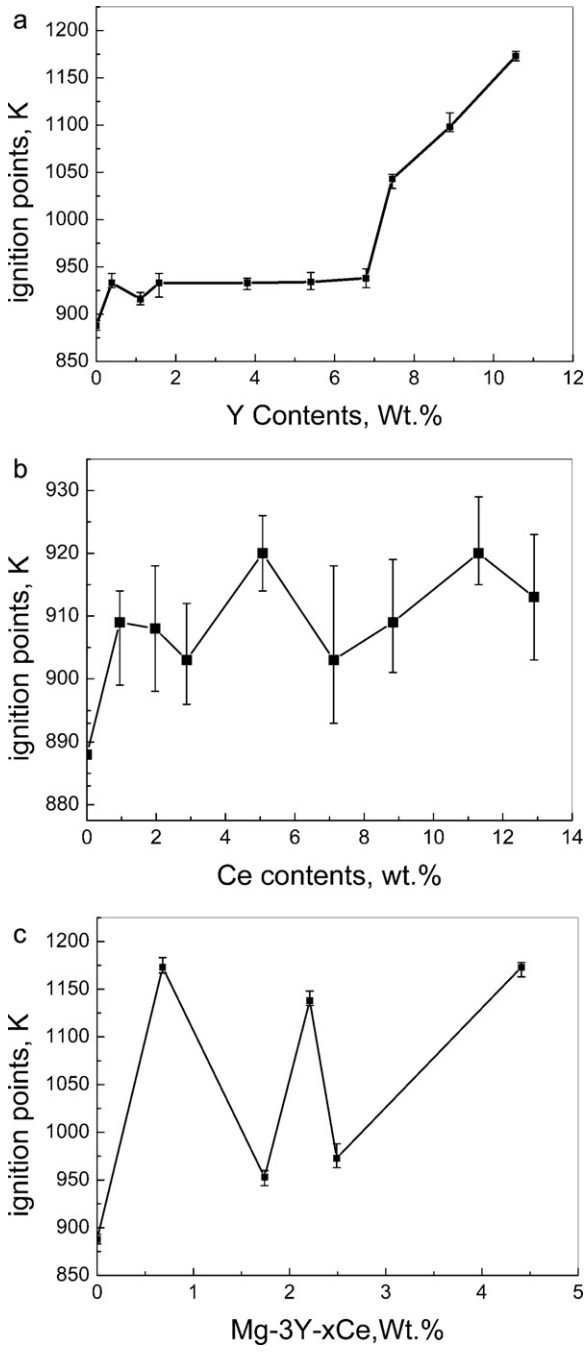

Fig. 3. Ignition points of magnesium alloys with different compositions: (a) Mg–Y alloys; (b) Mg–Ce alloys; (c) Mg–3Y–Ce alloys.

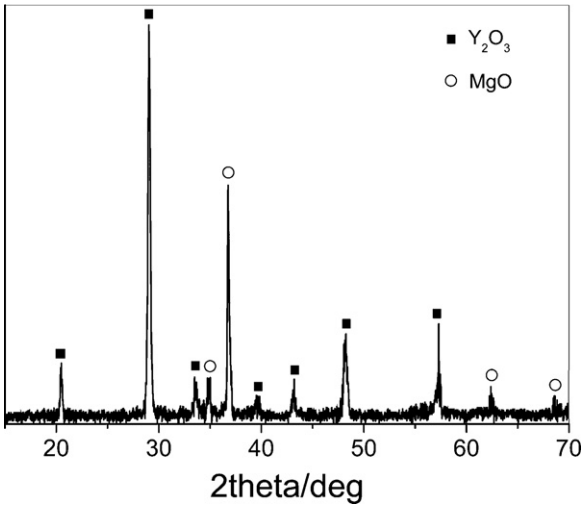

Fig. 4. X-ray diffraction patterns of oxide film formed on Mg–3Y–4.5Ce alloys oxidized for 0.5 h at 1173 K in air.

3.2. Microstructure and phase composition

In order to determine the oxidation products on the surface of molten Mg–Y–Ce ignition proof alloys, XRD analysis have been carried out, and Fig. 4 is the spectrum of the oxidation film of the Mg–3Y–4.5Ce alloys held at 1173 K for 0.5 h in the air. As a result, the oxidation film is composed of Y_2O_3 and MgO.

Table 1
EDS composition of the appointed areas in Fig. 5d.

Symbol	O content, at.%	Mg content, at.%	Y content, at.%	Ce content, at.%
1	57.66	10.51	31.17	0.66
2	10.49	86.81	2.60	0.10
3	47.54	1.60	50.86	0
4	26.71	72.52	0.77	0

Fig. 5 is SEM morphologies of the oxidation surface of Mg–3Y–4.5Ce alloy held at 1173 K for 0.5 h. The surface of Y_2O_3 film is rugged and compact (Fig. 5a and b). As seen in the cross-sectional images of the oxidation film (Fig. 5c and d), the oxidation film includes two layers. Referred to the results of XRD (Fig. 4) and EDS analysis (Table 1), the outer layer (symbol 1) is Y_2O_3, and the inner layer (symbol 2) is Mg and MgO with a little Y_2O_3.

In the oxidation course, to form Y_2O_3, Y element in the matrix near the interface diffuses into oxidation film, which is why Y content in position 4 is so little (Table 1). Ce element plays a role of the third element (seen in Section 4.3), which promotes the formation of Y_2O_3. It is unclear why nearly no Ce was detected (as Table 1) and the further experiment and analysis will be done in the next time.

3.3. AES analysis

AES analysis is carried out on the surface films of the Mg–3Y–4.5Ce alloys hold for 30 min at 1173 K in air. Fig. 6a is the AES differential spectrum of surface compositions. The oxidation surface (about 0.5–2 nm in depth) is composed of O, Mg, Y and Ce

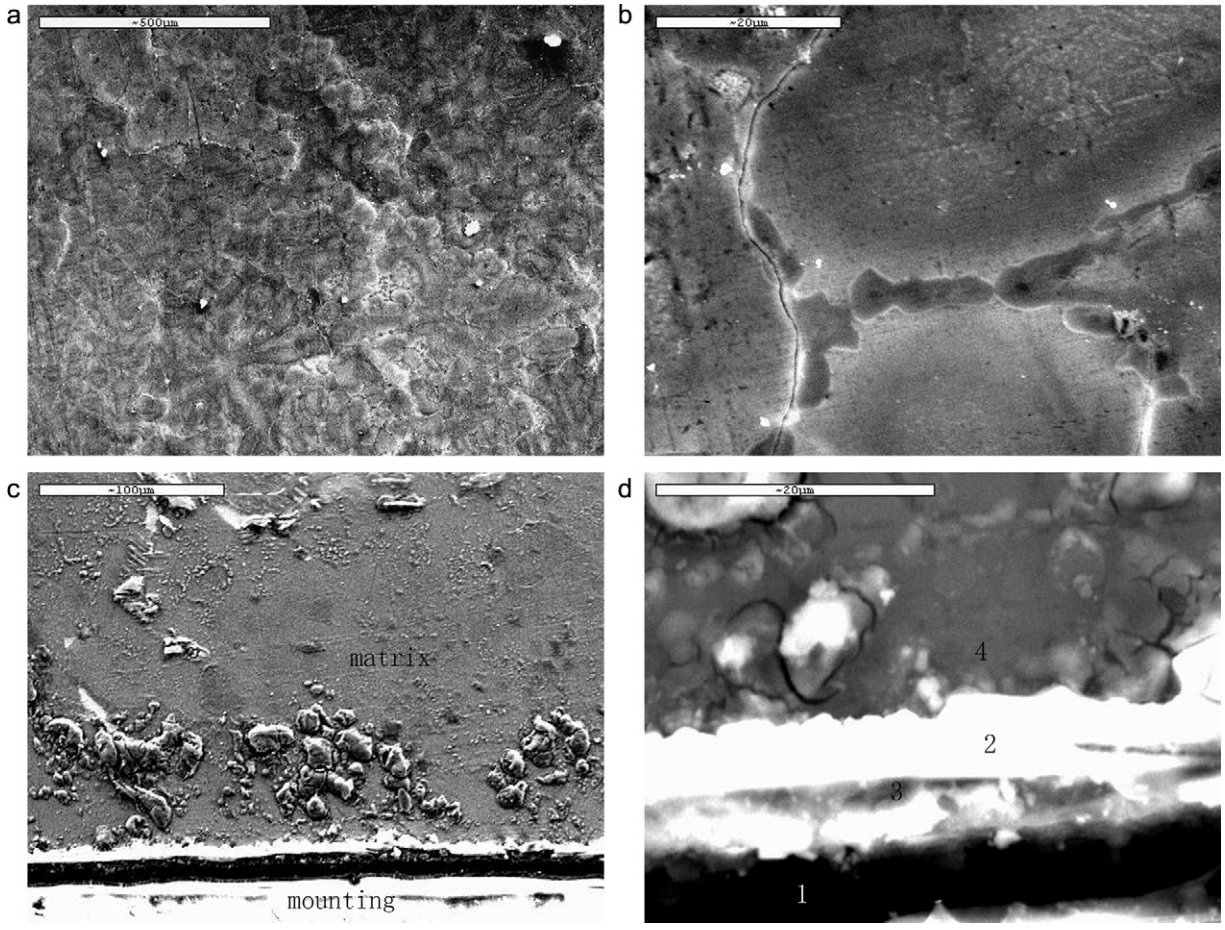

Fig. 5. SEM morphologies of the oxidation surface of Mg–3Y–4.5Ce alloy oxidized at 1173 K for 0.5 h: (a) oxidation surface (low magnified image); (b) oxidation surface (high magnified image); (c) the cross-sectional view of the oxidation film (low magnified image); (d) the cross-sectional view of the oxidation film (high magnified image).

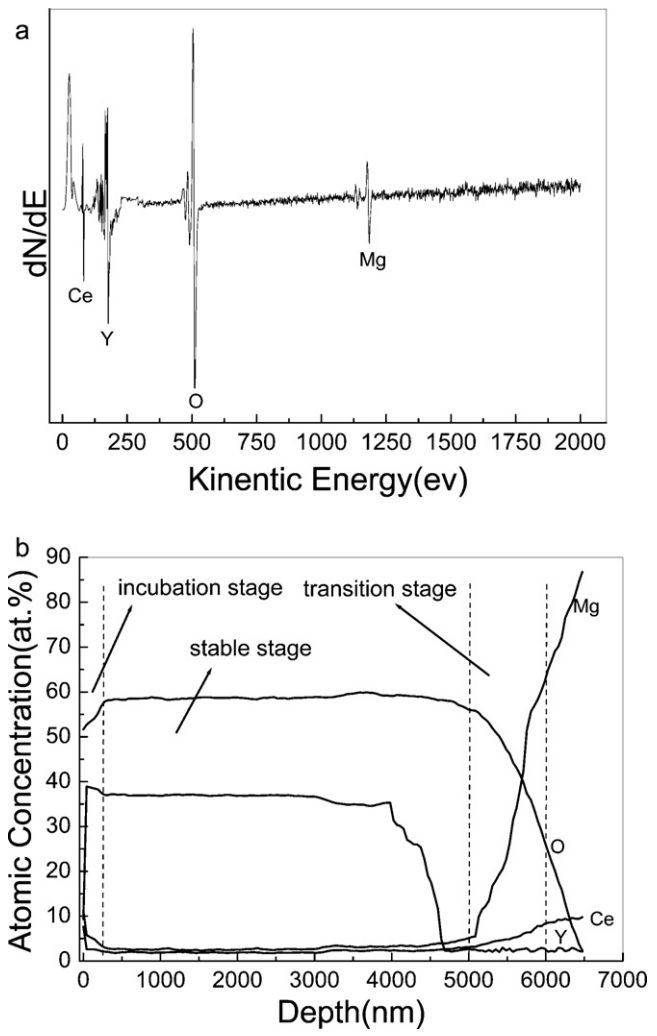

Fig. 6. AES surface analysis of oxidation films formed on Mg–3Y–4.5Ce alloy: (a) surface analysis; (b) in-depth AES profile.

elements, and the atom percentages of the four elements are shown in Table 2. Fig. 6b is the results of AES concentration–depth analysis of the elements, and there are several characteristics as follows:

- The changes of the elements concentration in depth undergo three stages: incubation stage, stable stage and transition stage. There exists a relatively stable stage for the concentration distribution of all elements. The conversion stage of element concentrations from surface to the stable stage is called as incubation stage, and the conversion stage of element concentrations from the stable layer to the matrix is called as transition layer. Moreover, the depth of stable layer is far more than those of the other two layers.
- In incubation stage, the contents of Mg and Ce elements are higher than those of Y and O elements. And the contents of Mg and Ce show downward trends while the concentrations of Y and O show upward trends.
- In stable stage, the total concentration of Y and O occupies more than 95 at.%, and there are very little Mg and Ce.

Table 2
Element concentration of oxidation films of Mg–3Y–4.5Ce alloy.

Elements	O	Mg	Y	Ce
Content, at.%	54.64	6.34	33.32	5.70

- In transition stage, concentration of Mg increases rapidly while those of O and Y decrease quickly. Moreover, concentration of Ce increases heavily.

It is presumed that there exist sesquioxide Y_2O_3 on the oxidation surface of molten Mg–3Y–4.5Ce alloys. Moreover, In the AES profile, the film thickness is identified by the content of O element. But in fact, the inner film includes some metal Mg. So the observed thickness (approx 13 μm, Fig. 5d) is bigger than the thickness identified by AES analysis (approx 6 μm, Fig. 6b).

4. Discussion

4.1. Thermodynamic analysis

The possible chemical reactions occurred on the surface of molten Mg–3Y–4.5Ce alloy are as follows:

$$2Mg(l) + O_2(g) = 2MgO \quad (1)$$

$$\frac{4}{3}Y(l) + O_2(g) = \frac{2}{3}Y_2O_3 \quad (2)$$

$$\frac{4}{3}Ce(l) + O_2(g) = \frac{2}{3}Ce_2O_3 \quad (3)$$

$$2Y(l) + 3MgO = Y_2O_3 + 3Mg(l) \quad (4)$$

$$2Ce(l) + 3MgO = Ce_2O_3 + 3Mg(l) \quad (5)$$

$$2Y(l) + Ce_2O_3 = Y_2O_3 + 2Ce(l) \quad (6)$$

The standard Gibbs free energy and the practical Gibbs free energy of the above reactions can be calculated using thermodynamic parameters. For simplification [13], the activity of Mg, Y and Ce are approximately replaced by their mole atomic concentrations, [Mg], [Y] and [Ce], respectively, and the activity of oxygen is approximately replaced by its volume fraction in air. Thus in Mg–3Y–4.5Ce alloy, $a_{MgO} = a_{CaO} = a_{Y_2O_3} = 1$, $a_{Mg} = [Mg]_{at.\%} = 0.9837$, $a_Y = [Y]_{at.\%} = 0.0083$, $a_{Ce} = [Ce]_{at.\%} = 0.008$, $a_{O_2} = [O_2]_{vol} = 0.25$. The standard Gibbs free energy and the practical Gibbs free energy of the reactions (1)–(6) can be calculated as follows:

$$p^0_{MgO} = \exp\frac{\Delta G^0_1}{RT} = 6.36 \times 10^{-46}\,Pa \quad (7)$$

$$\Delta G_1(1033\,K) = \Delta G^0_1 + RT\,\ln\left(\frac{1}{[Mg]^2_{at.\%} \cdot p_{O_2}}\right) = -881168.76 < 0\,J\,mol^{-1} \quad (8)$$

$$p^0_{Y_2O_3} = \exp\frac{\Delta G^0_2}{RT} = 1.9 \times 10^{-55}\,Pa \quad (9)$$

$$\Delta G_2(1033\,K) = \Delta G^0_2 + RT\,\ln\left(\frac{1}{[Y]^{4/3}_{at.\%} \cdot p_{O_2}}\right) = -101488.44 < 0\,J\,mol^{-1} \quad (10)$$

$$p^0_{Ce_2O_3} = \exp\frac{\Delta G^0_3}{RT} = 5.2 \times 10^{-52}\,Pa \quad (11)$$

$$\Delta G_3(1033\,K) = \Delta G^0_3 + RT\,\ln\left(\frac{1}{[Ce]^{4/3}_{at.\%} \cdot p_{O_2}}\right) = -946484.76 < 0\,J\,mol^{-1} \quad (12)$$

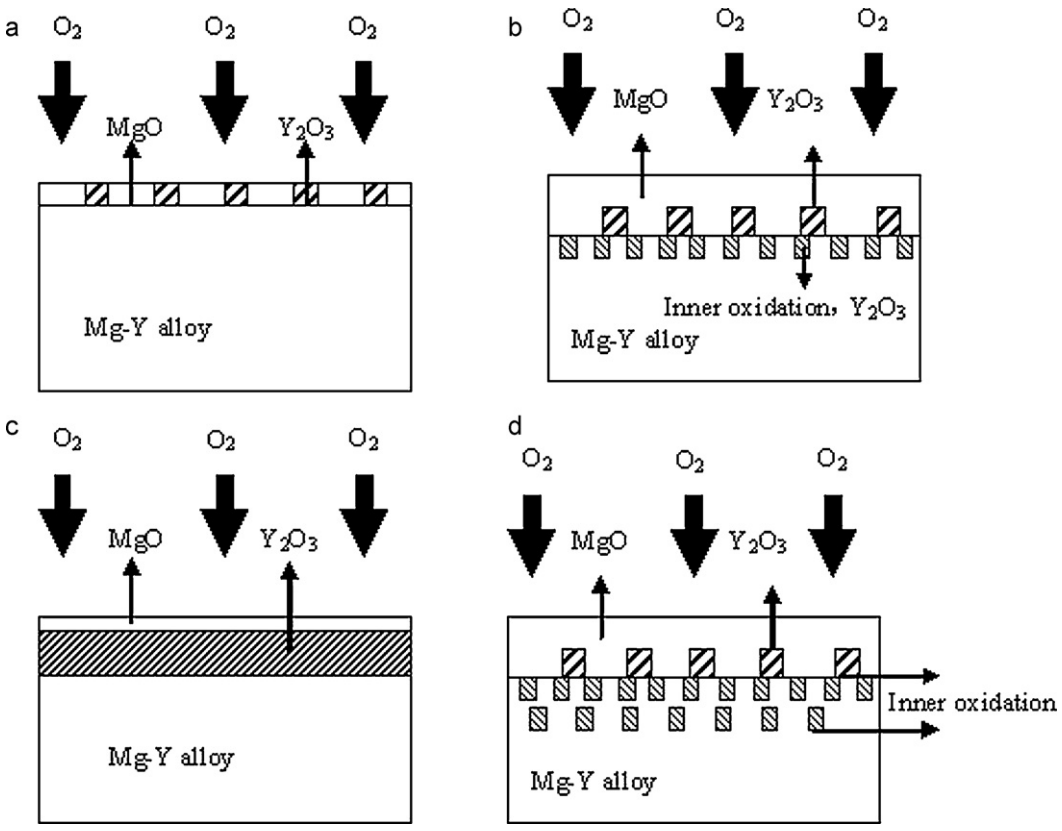

Fig. 7. (a–d) Schematic diagram of the selective oxidation course in Mg–Y alloy.

$$\Delta G_4(1033\,\mathrm{K}) = \Delta G_4^0 + RT\ln\left(\frac{[\mathrm{Mg}]_{\mathrm{at.\%}}^3}{[\mathrm{Y}]_{\mathrm{at.\%}}^2}\right) = -200543.68 < 0\,\mathrm{J\,mol^{-1}} \quad (13)$$

$$\Delta G_5(1033\,\mathrm{K}) = \Delta G_5^0 + RT\ln\left(\frac{[\mathrm{Mg}]_{\mathrm{at.\%}}^3}{[\mathrm{Ce}]_{\mathrm{at.\%}}^2}\right) = -97393.21 < 0\,\mathrm{J\,mol^{-1}} \quad (14)$$

$$\Delta G_6(1033\,\mathrm{K}) = \Delta G_6^0 + RT\ln\left(\frac{[\mathrm{Ce}]_{\mathrm{at.\%}}^2}{[\mathrm{Y}]_{\mathrm{at.\%}}^2}\right) = -102605.52 < 0\,\mathrm{J\,mol^{-1}} \quad (15)$$

The above calculations reveal that it is possible thermodynamically for reactions (1)–(6) occurring and the decomposition pressure of MgO, Y_2O_3 and Ce_2O_3 satisfy with a relation as: $p^0_{MgO}(6.36\times10^{-46}\,\mathrm{Pa}) > p^0_{Ce_2O_3}(5.2\times10^{-52}\,\mathrm{Pa}) > p^0_{Y_2O_3}(1.9\times10^{-55}\,\mathrm{Pa})$. Moreover, the XRD result (Fig. 4) reveals that there is no new complex oxide in the surface film of Mg–3Y–4.5Ce alloy, which indicates that MgO, Y_2O_3 and Ce_2O_3 cannot form solid solution with each other. According to thermodynamics principle [13], oxides with high decomposition pressure form in the outer layer with high oxygen partial pressure while the oxides with low decomposition pressure form in the inner layer with low oxygen partial pressure. In other words, the oxidation films of Mg–3Y–4.5Ce alloy should follow the following order: MgO at the outer layer, Ce_2O_3 at the medium layer and Y_2O_3 at the inner layer. Thus, the initial protective film has formed on the surface of Mg–3Y–4.5Ce alloy. In the subsequent oxidation process, Y_2O_3 layer may grow sequentially via the replacement reactions (4) and (6).

4.2. Selective oxidation model

According to the above analysis, a proposed mechanism for the high temperature oxidation of Mg–Y alloys is shown in Fig. 7. Thermodynamics suggests the initial stage is simultaneous oxidation of both Y and Mg (Fig. 7a). Gradually, the Y_2O_3 and the Mg matrix are covered by MgO as a result of the faster outward diffusion of Mg^{2+} than Y^{3+} (Fig. 7b). At this stage, because of the retardarce of the surface oxides the oxygen partial pressure on the interface of MgO/Mg matrix is decreased to be equal to decomposition pressure of MgO but larger than decomposition pressure of Y_2O_3. As a result, Y_2O_3 takes place by reaction (4). On the other hand, oxygen diffused through the Mg–Y alloy also makes Y oxidize at the interface of oxides/matrix. The both oxidations are called together as inner oxidation (Fig. 7b). If the inner oxides (Y_2O_3) form a continuous film (Fig. 7c) the inner oxidation will stop, and if any subsequent oxidation courses, only the Y_2O_3 film become thicker and thicker while Mg element does not oxidize further. As a result, the inner oxidation will be transformed as the outer oxidation and the velocity of oxidation will be decreased by reason of the retardarce of Y_2O_3 film. This is so-called selective oxidation. Conversely, if the inner oxides Y_2O_3 form discontinuous films (Fig. 7d), the oxygen partial pressure on the MgO/Mg interface will increase and the inner oxidation will continue, which means that the velocity of oxidation cannot be decreased and disastrous oxidation is inevitable.

From the above analysis, the key to selective oxidation is whether or not a continuous inner oxidation film is formed, which in turn depends on the concentration of alloying elements in the oxides/matrix interfaces. If the concentration of alloying elements

in the interface of oxides/matrix is larger, the continuous inner oxidation film is easier to form. Wagner [19] put forward a theoretical model to explain the transformation from inner oxidation to outer oxidation, and gave the critical concentration of the transition from internal to external scale formation as follows:

$$N_{B,min} > \sqrt{\frac{\pi g^*}{2\nu} N_O^S \frac{D_O V_M}{D_B V_{OX}}} \quad (16)$$

According to formula (16), when the concentration of alloying elements B is more than the critical concentration $N_{B,min}$, the volume fraction of the inner oxides BO will be larger than the critical volume fraction g^*. As a result, the discrete BO particles grow transversally and form a continuous inner oxidation film. For Mg–Y alloys, when the Y content is less than 7 wt%, there is no notable change for the ignition point of alloys, but as the Y concentrations increase continuously, the ignition points increase, and when the Y content is more than 10 wt%, alloys will not burn at 1173 K (Fig. 3). It is obvious that the critical concentration needed for selective oxidation in Mg–Y alloys is about 7 wt%. However, the critical concentration is only the minimum requirement for selective oxidation, and the higher concentration of Y is needed to form stable Y_2O_3 film. So when the content of Y is less than 10 wt%, even though the protective Y_2O_3 films formed initially, disastrous oxidation is inevitable because Y in the oxides/matrix interface will be consumed to less than 7 wt%. When the content of Y is more than 10 wt%, the Y concentration in the oxides/matrix interface will always be more than 7 wt%, so these alloys do not burn up to 1173 K.

The ignition points of Mg alloys depend mainly on two factors: the formation of the initial protective film and the regeneration of the protective film when it is destroyed. If the regeneration property of the protective film is poor, ignition points of the alloys depend on random conditions if or when the protective film is destroyed. Seen from Fig. 6b, there is a Y-depleted zone in the film/matrix interface, which can not provide enough Y elements for Y_2O_3 film to regenerate in time once it is destroyed, so the ignition points of Mg–Y–Ce alloys are unstable (Fig. 3) and are dependant on random conditions. In this paper, by using the special equipment (Fig. 1) the external factors which affect ignition points of alloys are eliminated as possible. And in our opinion, the damage of the protective film is mainly resulted from the cracking of the protective film itself. Now the cracking mechanism of the protective film is not yet clearly known.

4.3. The third-element effect

Seen from Fig. 3, due to addition of Ce element, the critical concentration of Y in Mg–Y alloys for forming protective film is decreased significantly. From the perspective of selective oxidation, with addition of trace Ce element the critical concentration N_B^0 of Y is reduced. This phenomenon also exists in other alloy systems and is called the third-element effect.

The third-element effect was explained qualitatively in Wagner's paper [16]. The third element was considered to play a role of "getter" which inhibits the diffusion of O to internal alloy so as to inhibit the inner oxidation of Y. For high temperature oxidation of Mg–Y–Ce alloys, MgO, Y_2O_3 and Ce_2O_3 initially form simultaneously. Then, if concentration of Ce is large enough a replacement reaction happens as follows:

$$2Ce(l) + 3MgO = Ce_2O_3 + 3Mg(l) \quad (17)$$

Thus, continuous Ce_2O_3 film forms on the surface of molten alloys, based on which the oxygen partial pressure on oxides/matrix interface is decreased and selective oxidation of Y was realized under the condition of smaller Y concentration. Thermodynamic analysis indicates that chemical activity of the third element must lay between that of the matrix element (Mg) and selective oxidation element (Y). Thermodynamics calculations show $0 > \Delta G^0_{MgO}(-893351) > \Delta G^0_{Ce_2O_3}(-1013648) > \Delta G^0_{Y_2O_3}(-1081630)$ which proves that Ce satisfies the necessary thermodynamics conditions to play the hypothesized role of the third element in the high temperature oxidation of Mg–Y alloys.

As the above analysis, Ce element plays a role of the third element, which promotes the formation of Y_2O_3. Moreover, although the structure analyses reveals that the surface film is composed by the outer layer and the inner layer (Mg and MgO), the outer layer (Y_2O_3) rather than the inner layer (Mg and MgO) is thought to play the role of preventing Mg alloys from vigorous oxidation or ignition. So the proposed model in Section 4.2 aims at explaining the formation mechanism of Y_2O_3 film.

5. Conclusions

1. When concentration of Y is larger than 10 wt%, ignition points of Mg–Y alloys increase markedly and the alloy do not ignite in air at 1173 K.
2. With the addition of Ce to Mg–Y the critical concentration of Y in Mg–Y alloys for forming protective film is decreased significantly.
3. XRD, SEM and AES analyses suggest that the protective films formed on the surface of Mg–Y–Ce alloys are mainly composed of Y_2O_3.
4. Based on the thermodynamics analysis, the selective oxidation model in Mg–Y system was established.
5. Analysis from the selective oxidation model of selective oxidation indicates that Ce play the role of "third elements".

Acknowledgments

The authors are grateful to the National Natural Science Foundation of China (50901048), the fund of the State Key Laboratory of Solidification Processing in NWPU (SKLSP201003), Program for the Top Young Academic Leaders of Higher Learning Institutions of Shanx and Natural Science Foundation of Shanxi (2010021022-5) for the financial support.

References

[1] X. Meng, R. Wu, M. Zhang, L. Wu, C. Chongliang, J. Alloys Compd. 486 (2009) 722.
[2] F.O. Méar, D.V. Louzguine-Luzgin, A. Inoue, J. Alloys Compd. 496 (2010) 149.
[3] N. Balasubramani, U.T.S. Pillai, B.C. Pai, J. Alloys Compd. 460 (2008) 6.
[4] P. Su, X. Wu, Y. Guo, Z. Jiang, J. Alloys Compd. 475 (2009) 773.
[5] W. Ha, Y.-J. Kim, J. Alloys Compd. 422 (2006) 208.
[6] G. Garces, P. Perez, P. Adeva, J. Alloys Compd. 387 (2005) 115.
[7] W. Ha, Y.J. Kim, J. Alloys Compd. 422 (2006) 208.
[8] X. Wang, W. Wu, Y. Tang, X. Zeng, S. Yao, J. Alloys Compd. 474 (2009) 499.
[9] F. Czerwinski, Acta Mater. 50 (2002) 2639.
[10] B.S. You, W.W. Park, I.S. Chung, Scr. Mater. 42 (2000) 1089.
[11] X.Q. Zeng, Q.D. Wang, Y.Z. Lu, W.J. Ding, Y.P. Zhu, C.Q. Zhai, X.P. Xu, Scr. Mater. 43 (2000) 403.
[12] N.V. Ravi Kumar, J.J. Blandin, M. Suery, E. Grojean, Scr. Mater. 49 (2003) 225.
[13] X.Q. Zeng, Q.D. Wang, Y.Z. Lu, W.J. Ding, Y.P. Zhu, C.Q. Zhai, C. Lu, X.P. Xu, Mater. Sci. Eng. A301 (2001) 154.
[14] N.V. Ravi Kumar, J.J. Blandin, M. Suery, E. Grosjean, Scr. Mater. 49 (2003) 225.
[15] J. Wang, R. Liao, L. Wang, Y. Wu, Z. Cao, L. Wang, J. Alloys Compd. 477 (2009) 341.
[16] X.M. Wang, X.Q. Zeng, Y. Zhou, G.S. Wu, S.S. Yao, Y.J. Lai, J. Alloys Compd. 460 (2008) 368.
[17] M. Liu, P. Schmutz, P.J. Uggowitzer, G. Song, A. Atrens, Corrosion Sci. 52 (2010) 3687.
[18] J.F. Fan, G.C. Yang, S.L. Cheng, H. Xie, W.X. Hao, M. Wang, Y.H. Zhou, Metall. Mater. Trans. 36A (2005) 235.
[19] C. Wagner, Z. Elektrochem. 63 (1959) 772.